

Multiconfiguration Dirac-Fock calculations on multi-valence-electron systems: Benchmarks on Ga-like ions

Feng Hu,^{1,2,*} Jiamin Yang,¹ Chuanke Wang,¹ Longfei Jing,¹ Shubo Chen,¹ Gang Jiang,² Hao Liu,² and Lianghuan Hao²

¹Research Center of Laser Fusion, China Academy of Engineering Physics, Mianyang, 621900 Sichuan, People's Republic of China

²Institute of Atomic and Molecular Physics, Sichuan University, Chengdu, 610065 Sichuan, People's Republic of China

(Received 8 July 2011; published 12 October 2011)

High-accuracy calculations of term energies and wavelengths of resonance lines in Ga-like ions have been performed as benchmarks in the request for accurate treatments of relativity, electron correction, and QED effects in multi-valence-electron systems. The calculated energy levels are in excellent agreement with the experimental results and the experimentally compiled energy values of the National Institute for Standards and Technology wherever available. The calculated values including core-valence correction are found to be in good agreement with other theoretical and experimental values for low- to medium- Z ions. On the basis of our calculations, some theoretical wavelengths for Ga-like Rb VII to Mo XII are also given. For higher- Z ions, computed wavelengths are compared well with the experimental results [E. Träbert, J. Clementson, P. Beiersdorfer, J. A. Santana, and Y. Ishikawa, *Phys. Rev. A* **82**, 062519 (2010), I. N Draganić *et al.*, *J. Phys. B* **44**, 025001 (2011)].

DOI: 10.1103/PhysRevA.84.042506

PACS number(s): 31.15.V–

I. INTRODUCTION

Ions of the gallium isoelectronic sequence have three valence electrons outside a closed $n = 3$ core and provide a model for studying the effects of the strong correlation on closely spaced levels in heavy atoms. Many examples in the Ga sequence of level crossings of states show the same parity and angular momentum. Such examples occur for both low and high nuclear charge Z . Notably, the $4s4p^2$ and $4s^24p$ levels become relatively more tightly bound as the nuclear charge Z increases. Such crossings provide stringent tests of atomic structure calculations. Comparisons with measurements of fine-structure splitting energies, transition rates, line strengths, and fine-structure intervals also provide useful tests of the different theoretical models.

For the energies of the $4s^24p$ and $4s4p^2$ states of Ga-like ions, there exist many experimental and theoretical studies. For low- to mid- Z ions ($Z \cong 30$ –54), the detailed theoretical investigation of radiative parameters for Br V–In XIX have been reported by Biémont by using the pseudorelativistic Hartree-Fock model combined with a semiempirical optimization of radial energy integrals [1]. This work is a summary of the experimental data corresponding to these ionization stages [2–15]. Some radiative lifetimes measured with beam-foil spectroscopy had been done for Br V [10], Kr VI [11–13], Ag XVII [14], and I XXIII [16], while spectra of the Rb VII–Mo XII ions emitted from sparks and laser-produced plasmas had been obtained by Litzén [15]. Ishikawa employed a relativistic R -matrix close-coupling method to study the energy levels of Kr VI [17].

For mid- to high- Z ions ($Z \cong 55$ –92), spectra of galliumlike rare-earth ions ($Z \cong 59$ –70) emitted from high-temperature low-density tokamak and high-density laser plasmas were recorded by Fournier *et al.* [18]. Recently, Utter *et al.* and Träbert carried out high-precision electron-beam ion-trap measurements of some resonance transitions in the x-ray spectra of highly charged Ga-like ions such as

W XLIV [19–21], Os XLVI [22], Au IL [23], Bi LII, Th LX, and U LXII [22]. On the theoretical front, Fournier calculated the transition wavelengths and oscillator strengths for W XLIV [24]. Later, Safronova and Safronova also reported the results for W XLIV by using the relativistic many-body perturbation theory method [25]. Quinet *et al.* [26] have carried out accurate calculations of the $4s^24p$ and $4s4p^2$ levels in the range $Z = 70$ –92 using the General-purpose Relativistic Atomic Structure Package (GRASP) developed by Norrington [27].

Our calculations are motivated by the need for accurate fine-structure data in a variety of scientific applications, which improve the understanding of the origin of these effects, allowing explanation of the existing results and further predictions. On the basis of our previous work [28,29], in this paper, besides the well-known problems arising from the necessity of considering some of the core electrons within the atom and the effects of electron correlation, relativity has to be taken into account in accurate calculations. The calculation methods used are based on the multiconfiguration Dirac-Fock (MCDF) method [30], as represented by the GRASPVU package (a general-purpose relativistic atomic structure package developed at Vanderbilt University). It is a modification and extension of the GRASP92 codes by Parpia *et al.* [31]. As shown in the current work, the MCDF optimal level (OL) mode, which has been applied successfully to a number of atomic systems and spectroscopic properties, is used to investigate the convergence of fine-structure transition rates, wavelengths, and line strengths in galliumlike ions ($32 \leq Z \leq 92$). The quality of the variational wave functions and the reliability of the calculated expectation values are assessed from the analysis of the convergence patterns as the approximate wave function is systematically improved, and from the comparisons with the available theoretical and experimental data.

The aim of the present paper is to extend our systematic approach to include new effects and to mainly concentrate on the low end of the sequence, where correlation effects are very important. We investigate the importance of core-valence correlation, which so far has been included explicitly in few of the calculations for Ga-like isoelectronic sequences. An

*hufengscu@139.com

important part of our approach is an attempt to study the level energies, wavelengths, and the QED corrections.

II. METHOD

A. MCDF

In the MCDF approach the wave function for a state labeled γJ , where γ represents the configuration and any other quantum numbers required to specify the state, is approximated by an expansion over jj -coupled configuration state functions (CSFs)

$$\Psi(\gamma J) = \sum_i C_i \Phi_i(\gamma_i J). \quad (1)$$

The configuration state functions $\Psi(\gamma J)$ are antisymmetrized linear combinations of products of relativistic orbitals,

$$\Phi(r) = \frac{1}{r} \begin{pmatrix} P_{n\kappa}(r)\chi_{\kappa m}(\vec{r}) \\ iQ_{n\kappa}(r)\chi_{-\kappa m}(\vec{r}) \end{pmatrix}. \quad (2)$$

Here κ is the relativistic angular momentum, $P_{n\kappa}(r)$ and $Q_{n\kappa}(r)$ are the large and small components of radial wave functions, respectively, and $\chi_{\kappa m}(\vec{r})$ is the spinor spherical harmonic in the lsj coupling scheme:

$$\chi_{\kappa m}(\vec{r}) = \sum_{m_l, m_s} \left\langle l \frac{1}{2} m_l m_s | j m \right\rangle Y_{l m_l}(\theta, \varphi) \xi_{m_s}(\sigma). \quad (3)$$

The radial functions $P_{n\kappa}(r)$ and $Q_{n\kappa}(r)$ are numerically represented on a logarithmic grid and are required to be orthonormal within each κ symmetry:

$$\int_0^\infty [P_{n'\kappa}(r)P_{n\kappa}(r) + Q_{n'\kappa}(r)Q_{n\kappa}(r)]dr = \delta_{n'n}. \quad (4)$$

In the multiconfiguration self-consistent field procedure, both the radial functions and the expansion coefficients for the configuration state functions are optimized to self-consistency.

B. Relativistic configuration interaction

Once a set of radial orbitals has been obtained, relativistic configuration interaction (RCI) calculations can be performed.

$$E_{n_a \kappa_a}^{\text{SE}} = \frac{(Z_a^{\text{eff}})^4}{\pi c^3 n^3} \times \begin{cases} F_{n_a \kappa_a}(Z_a^{\text{eff}}/c) & \text{for } 1s, 2s, 2p_{1/2}, \text{ and } 2p_{3/2} \text{ orbitals,} \\ F_{2\kappa_a}(Z_a^{\text{eff}}/c) & \text{for } ns, np_{1/2}, \text{ and } np_{3/2} \text{ orbitals,} \\ 0, & \text{otherwise.} \end{cases} \quad (7)$$

The use of Z^{eff} to roughly correct for electron screening is at best an expedient intended for inner shells where the orbitals are most likely to be nearly hydrogenic. It is likely to be increasingly less realistic as n increases.

Next in order of importance is the vacuum polarization correction. To lowest order, this is the short-range modification of the nuclear field due to screening by virtual electron-positron pairs. Expressions for the second- and fourth-order perturbation potentials that take fine nuclear size into account have been give in the literature, for example, in Ref. [35]. Only

Here only the expansion coefficients of the CSFs are determined. This is achieved by digitalizing the Hamiltonian matrix. In this implementation of the RCI program an iterative Davidson method is used together with a sparse matrix representation allowing for large expansions.

In the RCI calculations the transverse photon interaction may be included in the Hamiltonian:

$$H_{\text{trans}} = - \sum_{i < j} \left[\frac{\alpha_i \cdot \alpha_j}{R_{ij}} + (\alpha_i \cdot \nabla_i)(\alpha_j \cdot \nabla_j) \frac{\cos \omega_{ij} R_{ij}}{\omega_{ij}^2 R_{ij}} \right], \quad (5)$$

where photon frequency ω_{ij} used by the RCI program in calculating the matrix elements of the transverse photon interaction is taken to be the difference in the diagonal Lagrange multipliers and associated with the orbitals. In general, diagonal Lagrange multipliers are approximate electron-removal energies only when orbitals are spectroscopic and singly occupied. Thus it is not known how well the code can determine the full transverse photon interaction when correlation orbitals are present. What can be obtained instead is the low-frequency limit $\omega_{ij} \rightarrow 0$, usually referred to as the Breit interaction.

C. QED

There are two major components in the QED correction [32]. Known simply as self-energy, the dominant correction to energy arises from the lowest-order modification to an electron's interaction with quantized ambient electromagnetic field when in the presence of the field due to the nucleus and the other atomic electrons. In terms of a function $F_{n\kappa}^{\text{SE}}$ that varies slowly with respect to its argument, the self-energy in hydrogenlike systems is given by

$$F_{n\kappa}^{\text{SE}}(Z/c) = \frac{Z^4}{\pi c^3 n^3} F_{n\kappa}(Z/c). \quad (6)$$

Tabulations of $F_{n\kappa}(Z/c)$ for the $1s, 2s, 2p_{1/2}$, and $2p_{3/2}$ states in these one-electron systems are given in the literature [33,34]. In GRASPVU, a rough estimate of the self-energy is obtained by setting

diagonal contributions,

$$H_{rr}^{\text{VP}} = \sum_{a=1}^{n_w} q_r(a) \int_0^\infty dr V^{VP}(r) [P_{n_a \kappa_a}^2(r) + Q_{n_a \kappa_a}^2(r)], \quad (8)$$

from these potentials have been included in this version of GRASPVU.

D. Generation of configuration expansions

In this work, we included different correlations into the calculation in a systematic approach. The correlation energy

is defined as the energy difference between the exact solution to the Dirac equation and the Dirac-Fock (DF) solution. The contribution from different types of correlation then can be defined as the energy difference between the solution including the particular correlation under investigation and the DF solution. To classify the correlation, the atomic electrons can be divided into two parts: valence electrons and core electrons. As a result, the correlation between the valence electrons is defined as valence (VV) correlation, and the correlation between the valence electrons and core electrons is defined as core-valence (CV) correlation. The remaining correlation is core-core (CC) correlation, which describes the correlation between the core electrons.

It is, from some perspectives, desirable to perform separate calculations for each of the studied atomic states. This approach, however, is impractical and time consuming. Instead, the atomic state functions for a number of closely spaced levels were determined together in the so-called extended optimal level (EOL) procedure. To account for the close degeneracy between $4s4p^2$ and $4s^24p$, the atomic state functions for $4s4p^2\ ^2S_{1/2}$, $4s4p^2\ ^4P_{1/2,3/2,5/2}$, $4s4p^2\ ^2D_{3/2,5/2}$, and $4s^24p^2\ P_{1/2,3/2}$ were determined simultaneously. In the remaining cases atomic state functions for levels belonging to the same configuration were grouped together.

In the MCDF approach, the correlation is represented by different constraints on the generation of the CSFs included in Eq. (1). If we only include the VV correlation, the core electrons are kept fixed in all the CSFs generated. To include the CV correlation, we allow one of the core electrons to be excited to generate the CSFs. Finally, the CC correlation can be taken into account by allowing more than one core electron to be excited.

E. Calculation procedure

As a starting point, MCDF calculations in the EOL scheme were performed for each group of atomic states using configuration expansions including all lower states of the same J symmetry and parity, and a Dirac-Coulomb version was used, for the optimization of the orbitals, including Breit corrections in a final configuration interaction calculation. To build a CSF expansion, restrictive active space methods were also used. The idea of the active space methods is to consider only electrons from the active space and to excite them from the occupied orbitals to the unoccupied ones. The orbital was increased systematically in order to monitor the convergence of the calculation. Since the orbitals with the same principal quantum number n often have similar energies, the active set is usually enlarged in steps of orbital layers. It is convenient to refer to the $\{1s, 2s, 2p, 3s, 3p, 3d\}$ set of orbitals as the $n = 3$ orbital layer, $\{1s, 2s, 2p, \dots, 4s, 4p, 4d, 4f\}$ as the $n = 4$ layer, etc. Larger orbital sets can result in a considerable increase of computational time required for the problem, and appropriate restrictions may be necessary. We divided the calculations into two parts, one where we optimized a set of orbitals for the even states and one for the odd states; i.e., the upper and lower states were described by two independently optimized sets of orbitals. Because of this we had to use biorthogonal transformation [36] of the atomic state functions to calculate the transition parameters.

In our calculations, we generate the CSFs using the active space approach, and we do this by exciting electrons from the spectroscopic reference configuration to a set of orbitals called the active set (AS). The active set is a set of orbitals which are all orbitals except those common to all CSFs, and it defines the CSFs included in the atomic state function (ASF). We increase the AS in a systematic way to ensure the convergence of the atomic parameters under consideration.

Some tests were undertaken for Ge II, to determine what sort of corrections are necessary to be included in our calculation. First, we only included the VV correlation. In subsequent calculations, the CV correction due to the $3d$, $3p$, and $3s$ orbitals was successively included. The results of these tests show that the CV correction makes significant changes to the calculations and cannot be ignored. Furthermore, the largest contribution is due to the CV correction from the $3d$ orbitals, and the correction from the $3s$ and $3p$ CV correction is very small. Thus, like our previous papers [28,29], we only include the CV correction of the $3d$ orbitals in calculation. The case of CC correction is similar to that for CV; that is, only the corrections from $3d$ orbitals are considered.

A similar calculation procedure was previously introduced by one of our authors [28]; here, we only give an outline. For Ga-like ions, the ground and first excited configurations are $4s^24p$, $J = 1/2$, and $4s4p^2$, respectively. In the first step, the active set is

$$AS1 = \{4s, 4p, 4d, 4f\}. \quad (9)$$

Then, we increase the active set in the following way:

$$AS2 = AS1 + \{5s, 5p, 5d, 5f, 5g\}, \quad (10)$$

$$AS3 = AS2 + \{6s, 6p, 6d, 6f, 6g\}, \quad (11)$$

$$AS4 = AS3 + \{7s, 7p, 7d, 7f, 7g\}. \quad (12)$$

The VV, CV, and CC corrections used different active sets; here we discuss each clearly. Here, in our VV method, we set $1s^22s^22p^63s^23p^63d^{10}$ as our core electrons in the calculation. Then we considered increasing the principal quantum number n , and optimized the orbitals AS1, AS2, AS3, and AS4. In the CV model, the core electrons are $1s^22s^22p^63s^23p^63d^9$; then we optimized the layer by n . We generated the CSFs of the form of $1s^22s^22p^63s^23p^63d^9ASn$, $n = 1-3$. For the CC method, wave functions were generated by $1s^22s^22p^63s^23p^63d^8ASn$, $n = 1$ or 2 .

III. RESULTS AND DISCUSSION

The success of a calculation relies on a judiciously chosen configuration expansion. To ensure the convergence of a calculated expectation value within a certain correlation model, the configuration expansion must be enlarged in a systematic way. A very efficient way of doing this is to use the active set approach, where jj -coupled configuration state functions of a specified parity P and angular momentum J symmetry are generated by excitations from one or more reference configurations to an active set of orbitals. The convergence of the atomic property can then be studied as a function of the size of the active set. To build a reasonable correlation model and control the accuracy, we performed tentative calculations

TABLE I. Possible three-particle states in the $n = 4$ complex.

J	jj coupling	LS coupling
1/2	$4p_{1/2}4p_{1/2}[0]4s_{1/2}$	$4s4p^2\ ^4P$
1/2	$4p_{1/2}4p_{3/2}[1]4s_{1/2}$	$4s4p^2\ ^2S$
1/2	$4p_{3/2}4p_{3/2}[0]4s_{1/2}$	$4s4p^2\ ^2P$
3/2	$4p_{1/2}4p_{3/2}[1]4s_{1/2}$	$4s4p^2\ ^4P$
3/2	$4p_{1/2}4p_{3/2}[2]4s_{1/2}$	$4s4p^2\ ^2D$
3/2	$4p_{3/2}4p_{3/2}[2]4s_{1/2}$	$4s4p^2\ ^2P$
5/2	$4p_{1/2}4p_{3/2}[2]4s_{1/2}$	$4s4p^2\ ^4P$
5/2	$4p_{3/2}4p_{3/2}[2]4s_{1/2}$	$4s4p^2\ ^2D$
1/2	$4s_{1/2}4s_{1/2}[0]4p_{1/2}$	$4s^24p\ ^2P$
3/2	$4s_{1/2}4s_{1/2}[0]4p_{3/2}$	$4s^24p\ ^2P$

on transition energies and line strengths of the $4s^24p-4s4p^2$ $E1$ transition for the Ga-like isoelectronic sequence.

To assist readers in identifying energy levels and locating transitions, we present schematic energy levels, with their labels (both jj and LS designations), for Ga-like ions in Table I. When starting calculations from relativistic Dirac-Fock wave functions, it is natural to use the jj designations for uncoupled transition and energy matrix elements.

In the calculations, the states of the $4s^24p$ and $4s4p^2$ configurations were optimized layer by layer in an EOL scheme. These calculations were followed by calculations with CSF expansions generated by single (S) and double (D) excitations from the $4s$ and $4p$ shells of the reference configurations $4s^24p$ and $4s4p^2$ to the active set in order to consider VV correlations. The active set was systematically increased by adding layers of new orbitals. The largest active set included all relativistic orbitals with $n \leq 7$ and $l \leq 4$. Due to stability problems in the self-consistent field procedure, the optimization of radial orbitals was done layer by layer (see Table II). Breit interaction as a part of the electron correlations has been taken into account by a RCI calculation in each step. All the results listed here have considered the QED corrections, which are discussed later.

Table II displays the experimental energy levels [37] and the computed transition energies as functions of the increasing

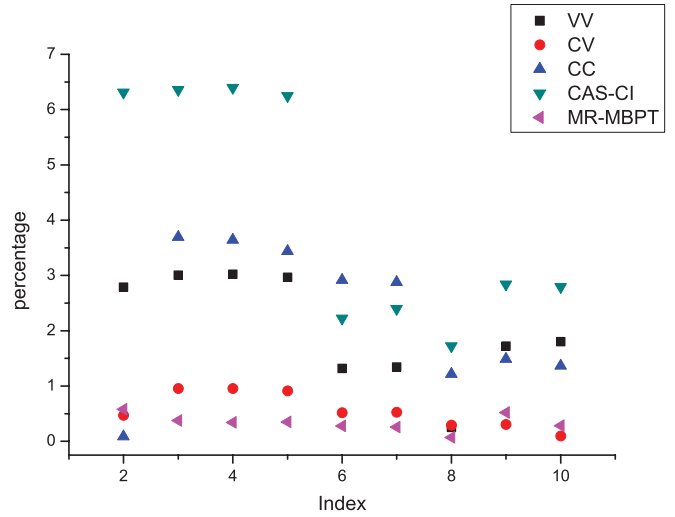


FIG. 1. (Color online) Differences between the available theoretical and experimental values and the present values for a fine structure of Kr^{5+} ; the index numbers correspond to the levels listed in Table II.

active sets and multireference sets for Kr^{5+} . The first column in the table represents the largest principal quantum number of the active set involved in each step of the calculation. As can be seen from Table II, the VV correlations have converged when $n = 7$, whereas for CV and CC, the principal number has been limited to $n = 6$ and $n = 5$, respectively. This is because, first, from Table II, we can find that the contribution from $n = 7$ orbitals is less than 0.02%. Second, the number of the CSFs would increase very rapidly when we consider the $3d$ orbitals, so it is very difficult to get convergence. Also because of the computer calculation limit and the problem of the program GRASPVU itself, we did not compare the VV, CV, and CC models on an equal footing, as mentioned above. The experimental results are obtained from Ref. [37]. The other two calculated results are from Ishikawa and Vilkas, who used the method of a complete active space configuration interaction (CASCI) and a relativistic R -matrix close-coupling method based on the relativistic multireference many-body perturbation theory (MRMBPT) [17]. From Table II, we

 TABLE II. Comparison with experiment of the calculated term energies (cm^{-1}) in galliumlike Kr (Kr^{5+}).

Index	Level	Valence correction				Core-valence corrections			Core-core corrections		Expt. ^a	Other calculations	
		$n = 4$	$n = 5$	$n = 6$	$n = 7$	$n = 4$	$n = 5$	$n = 6$	$n = 4$	$n = 5$		CASCI ^b	MRMBPT ^b
1	$4s^24p\ ^2P_{1/2}$	0	0	0	0	0	0	0	0	0	0	0	0
2	$4s^24p\ ^2P_{3/2}$	7 834	7 882	7 883	7 883	7 886	8 074	8 072	8 091	8 102	8 110	7 598	8 157
3	$4s4p^2\ ^4P_{1/2}$	103 445	104 476	104 571	104 595	109 052	106 465	106 810	100 025	103 851	107 836	100 979	108 238
4	$4s4p^2\ ^4P_{3/2}$	106 659	107 709	107 806	107 831	112 268	109 789	110 135	103 294	107 142	111 193	104 080	111 574
5	$4s4p^2\ ^4P_{5/2}$	110 902	111 930	112 026	112 051	116 518	114 097	114 429	107 724	111 506	115 479	108 262	115 880
6	$4s4p^2\ ^2D_{3/2}$	139 906	139 841	139 814	139 807	145 959	142 331	142 400	149 043	145 805	141 672	138 525	142 067
7	$4s4p^2\ ^2D_{5/2}$	140 997	140 865	140 820	140 807	147 018	143 414	143 472	149 970	146 831	142 727	139 304	143 093
8	$4s4p^2\ ^2S_{1/2}$	171 475	170 815	170 552	170 512	177 702	170 904	170 579	173 936	172 149	170 084	173 014	170 203
9	$4s4p^2\ ^2P_{1/2}$	183 886	183 283	183 157	183 136	189 876	180 849	180 584	187 864	182 716	180 039	185 151	179 105
10	$4s4p^2\ ^2P_{3/2}$	187 834	187 260	187 148	187 129	193 781	184 220	183 993	192 140	186 324	183 817	188 949	183 299

^aTaken from Ref. [37].

^bTaken from Ref. [17].

TABLE III. Energy levels (in cm^{-1}) for Ge II, As III, Se IV, Br V, Kr VI, and Rb VII compared with NIST [37] experimental data.

Configuration	Level	Level (cm^{-1})				Difference(%)		
		VV	CV	CC	NIST	VV ^a	CV ^b	CC ^c
				Z = 33				
4s ² 4p	² P _{1/2}	0	0	0	0			
	² P _{3/2}	2 788	2 911	2 942	2 940	-5.15	-0.96	0.10
4s4p ²	⁴ P _{1/2}	62 246	64 418	60 973				
	⁴ P _{3/2}	63 355	65 574	62 131				
	⁴ P _{5/2}	64 985	67 263	63 861				
	² D _{3/2}	82 995	86 560	90 032	85 310	-2.71	0.29	5.53
	² D _{5/2}	83 326	87 060	90 451	85 633	-2.69	0.50	5.63
	² S _{1/2}	105 792	108 134	109 413	107 808	-1.87	0.30	1.49
	² P _{1/2}	107 249	114 093	116 348	113 936	-5.87	0.14	2.11
	² P _{3/2}	116 771	115 703	118 027	115 424	1.17	0.24	2.26
				Z = 34				
4s ² 4p	² P _{1/2}	0	0	0	0			
	² P _{3/2}	4 197	4 350	4 370	4 376	-4.08	-0.58	-0.12
4s4p ²	⁴ P _{1/2}	76 220	78 987	75 122	79 395	-3.99	-0.51	-5.38
	⁴ P _{3/2}	77 893	80 821	76 843	80 980	-3.81	-0.19	-5.10
	⁴ P _{5/2}	80 261	82 961	79 320	83 589	-3.98	-0.75	-5.10
	² D _{3/2}	102 061	105 177	108 520	104 211	-2.06	0.92	4.13
	² D _{5/2}	102 548	105 720	109 067	104 706	-2.06	0.96	4.16
	² S _{1/2}	128 163	129 212	130 566	128 787	-0.48	0.33	1.38
	² P _{1/2}	138 236	136 294	138 480	136 134	1.54	0.11	1.72
	² P _{3/2}	140 625	138 500	140 790	138 354	1.64	0.10	1.76
				Z = 35				
4s ² 4p	² P _{1/2}	0	0	0	0			
	² P _{3/2}	5 886	6 058	6 081	6 090	-3.34	-0.52	-0.13
4s4p ²	⁴ P _{1/2}	90 327	92 514	89 409				
	⁴ P _{3/2}	92 701	94 963	91 835				
	⁴ P _{5/2}	95 932	98 267	95 188				
	² D _{3/2}	120 897	123 700	127 066	122 941	-1.66	0.61	3.35
	² D _{5/2}	121 599	124 462	127 809	123 628	-1.64	0.67	3.38
	² S _{1/2}	149 414	149 955	151 414				
	² P _{1/2}	160 686	158 361	160 511	158 158	1.59	0.12	1.48
	² P _{3/2}	163 861	161 171	163 472	161 011	1.77	0.09	1.52
				Z = 36				
4s ² 4p	² P _{1/2}	0	0	0	0			
	² P _{3/2}	7 883	8 072	8 102	8 110	-2.78	-0.46	-0.08
4s4p ²	⁴ P _{1/2}	104 595	106 810	103 851	107 836	-3.00	-0.95	-3.69
	⁴ P _{3/2}	107 831	110 135	107 142	111 193	-3.02	-0.95	-3.64
	⁴ P _{5/2}	112 051	114 429	111 506	115 479	-2.96	-0.90	-3.44
	² D _{3/2}	139 807	142 400	145 805	141 672	-1.31	0.51	2.91
	² D _{5/2}	140 807	143 472	146 831	142 727	-1.34	0.52	2.87
	² S _{1/2}	170 512	170 579	172 149	170 084	0.25	0.29	1.21
	² P _{1/2}	183 136	180 584	182 716	180 039	1.72	0.30	1.48
	² P _{3/2}	187 129	183 993	186 324	183 817	1.80	0.09	1.36
				Z = 37				
4s ² 4p	² P _{1/2}	0	0	0	0			
	² P _{3/2}	10 218	10 422	10 461	10 467	-2.37	-0.42	-0.05
4s4p ²	⁴ P _{1/2}	119 045	121 291	118 465	122 251	-2.62	-0.78	-3.09
	⁴ P _{3/2}	123 328	125 679	122 809	126 679	-2.64	-0.78	-3.05
	⁴ P _{5/2}	128 667	131 089	128 317	132 078	-2.58	-0.74	-2.84
	² D _{3/2}	158 947	161 382	164 837	160 699	-1.09	0.42	2.57
	² D _{5/2}	160 351	162 880	166 258	162 196	-1.13	0.42	2.50
	² S _{1/2}	191 613	191 222	192 897	190 700	0.47	0.27	1.15
	² P _{1/2}	205 831	203 164	205 290	202 859	1.46	0.15	1.19
	² P _{3/2}	210 655	207 153	209 524	206 942	1.79	0.10	1.24

^aDifferences were computed according to $(\text{VV-NIST}) \times 100/\text{NIST}$.^bDifferences were computed according to $(\text{CV-NIST}) \times 100/\text{NIST}$.^cDifferences were computed according to $(\text{CC-NIST}) \times 100/\text{NIST}$.

TABLE IV. Energy levels (in cm^{-1}) for Sr VIII to Nb XI.

Configuration	Level	Level (cm^{-1})				Splitting (cm^{-1})				
		VV	CV	CC	Ref. [9]	VV	CV	CC	Ref. [9]	Ref. [1]
$Z = 38$										
$4s^2 4p$	$^2P_{1/2}$	0	0	0	0					
	$^2P_{3/2}$	12 920	13 140	13 188	13 198	12 920	13 140	13 188	13 198	13 199
$4s 4p^2$	$^4P_{1/2}$	133 695	136 969	133 266	137 002					
	$^4P_{3/2}$	139 238	142 698	138 878	142 730	5 543	5 729	5 612	5 728	5 760
	$^4P_{5/2}$	145 824	148 290	145 664	149 356	6 586	6 786	6 786	6 626	6 592
	$^2D_{3/2}$	178 421	180 730	184 239	180 074					
	$^2D_{5/2}$	180 367	182 801	186 195	182 164	1 946	2 071	1 956	2 090	1 917
	$^2S_{1/2}$	212 820	211 983	213 752	211 438					
	$^2P_{1/2}$	228 958	226 255	228 384	225 984					
	$^2P_{3/2}$	234 601	230 794	233 211	230 550	5 643	4 538	4 827	4 566	4 562
$Z = 39$										
$4s^2 4p$	$^2P_{1/2}$	0	0	0	0					
	$^2P_{3/2}$	15 947	16 221	15 829	16 322	15 947	16 221	15 829	16 322	16 324
$4s 4p^2$	$^4P_{1/2}$	142 155	153 793	149 580	151 878					
	$^4P_{3/2}$	149 006	160 578	156 371	159 150	6 851	6 785	6 791	7 272	7 301
	$^4P_{5/2}$	156 972	168 481	164 277	167 130	7 965	7 903	7 906	7 980	7 926
	$^2D_{3/2}$	197 538	199 086	205 590	199 863					
	$^2D_{5/2}$	199 821	201 920	207 534	202 731	2 282	2 834	1 944	2 868	2 677
	$^2S_{1/2}$	230 367	232 308	238 535	232 367					
	$^2P_{1/2}$	249 673	249 644	255 332	249 556					
	$^2P_{3/2}$	254 302	254 963	260 967	254 745	4 628	5 319	5 635	5 189	5 085
$Z = 40$										
$4s^2 4p$	$^2P_{1/2}$	0	0	0	0					
	$^2P_{3/2}$	19 560	19 816	19 881	19 884	19 560	19 816	19 881	19 884	19 884
$4s 4p^2$	$^4P_{1/2}$	163 632	165 954	163 476	166 984					
	$^4P_{3/2}$	172 467	174 969	172 399	176 081	8 835	9 015	8 923	9 097	9 129
	$^4P_{5/2}$	181 915	184 464	182 130	185 524	9 448	9 495	9 731	9 443	9 372
	$^2D_{3/2}$	218 679	220 786	224 406	220 143					
	$^2D_{5/2}$	222 269	224 598	228 002	224 022	3 590	3 812	3 596	3 879	3 665
	$^2S_{1/2}$	255 835	254 173	256 090	253 571					
	$^2P_{1/2}$	276 099	274 474	276 622	273 979					
	$^2P_{3/2}$	281 270	279 998	282 513	279 655	5 171	5 524	5 891	5 676	5 580
$Z = 41$										
$4s^2 4p$	$^2P_{1/2}$	0	0	0	0					
	$^2P_{3/2}$	23 570	23 845	23 918	23 928	23 570	23 845	23 918	23 928	23 929
$4s 4p^2$	$^4P_{1/2}$	178 932	181 271	178 898	182 296					
	$^4P_{3/2}$	189 872	192 427	189 939	193 561	10 940	11 156	11 041	11 265	11 294
	$^4P_{5/2}$	200 921	203 506	201 323	204 563	11 049	11 079	11 384	11 002	10 924
	$^2D_{3/2}$	239 589	241 610	245 284	240 973					
	$^2D_{5/2}$	244 367	246 678	250 071	246 140	4 778	5 068	4 787	5 167	4 935
	$^2S_{1/2}$	277 770	275 739	277 710	275 120					
	$^2P_{1/2}$	302 366	299 621	301 984	299 278					
	$^2P_{3/2}$	310 221	305 777	308 344	305 396	7 855	6 156	6 360	6 118	6 035

can see that the core-valence correlation is important in determining the energy of the calculated levels. In order to see the correction clearly, the differences between the calculated and the experimental results are plotted in Fig. 1. The deviation from experiment of the CASCI energies reaches up to 7100 cm^{-1} . The term energies calculated with the MRMBPT deviate from experiment on the order of 100 cm^{-1} for most of the excited levels. Our CV results are found to be close to the MRMBPT results. Compared with the experimental results, the maximum difference is only 0.95%.

In Table III, computed energies for Ge II, As III, Se IV, Br V, Kr VI, and Rb VII are compared with the experimental data recommended by the NIST [37]. Three calculations are presented for each ion. For the most part, there is improvement in the agreement with experiment when core orbital replacements are included. This corresponds to less than 1% of the energies of energy levels belonging to $4s^2 4p$ and $4s 4p^2$ (Table III). From Table III it is clear that the CV correlation results show excellent agreement with the NIST data. The computed results for $4s 4p^2 \ ^2P_{3/2}$ calculated by the

TABLE V. Convergence of the length (S_l) and velocity (S_v) line strength and transition energy between the $4s^24p^2P_{1/2}-4s4p^2^2S_{1/2}$ configuration of Ga-like Br.

AS ^a	VV			CV			CC		
	S_l	S_v	λ (Å)	S_l	S_v	λ (Å)	S_l	S_v	λ (Å)
4	1.27	1.29	664.820	1.26	1.29	666.491	1.26	1.43	666.283
5	1.29	1.32	667.813	1.30	1.35	667.368	1.33	1.52	666.441
6	1.29	1.35	669.078	1.32	1.35	668.864			
7	1.30	1.37	669.281						
Obs ^b			668.918						

^aAS, active set, specified by the n value.^bReference [38].

MCDF CC model are in a better agreement with the NIST data. This agreement is slightly spurious in that all the energy-level values reported in this paper are uncorrected for the observed ground-level energies to the calculated energies.

The computed energies and fine-structure splitting for Sr VII, Y IX, Zr X, and Nb XI are compared with the experimental results given by Litzén and Reader [15] and the semiempirical results recommended by Biémont and Qunit [1]. The fine-structure splitting of the states also improves slightly with the inclusion of core correlations. Relative to the ground states, the energies of other states are up to about 900 cm^{-1} in error. This corresponds to less than 1% of the energies of the levels. It is clear that the CV correlation results show excellent agreement with experimental values within 0.64%. The energy-level splitting listed in the last column of Table IV is calculated by using the data given in Ref. [1]. A more detailed comparison of the calculated and experimental energies for these levels (Table IV) indicates that some splittings given by our GRASPVU calculation are in better agreement with experimental energies than the semiempirical results. Especially, the maximum difference in energy-level splitting between the results of the experiment and our CV results is 1.18%, but the maximum difference for the semiempirical results and experimental results is 6.59%. In the work presented here we have increased the number of configurations or the size of the orbital set in

a systematic manner until good convergence was obtained. This difference in the three modes should account for a large fraction of the disagreement in the results. From Tables III and IV it is clear that the fine structure for this term is highly irregular along the sequence and it is not described very well in the present calculations. The fine-structure splitting is strongly affected by the multireference set and it would be desirable to increase it further.

In Table V the line strengths for $4s^24p^2P_{1/2}-4s4p^2^2S_{1/2}$ in Br V are shown as functions of increasing active sets and multireference sets. The results are from the various valence and core-valence correlation calculations. The convergence of the results is clearly seen as n increases in the two correlation calculations. As can be seen from this table, the agreement of the two gauges is very good and the near-equal values of the length and velocity of the transitions give an additional check on the accuracy of our results. And the agreement of the two gauges improves with increasing n . At the same time, we can find that the length value is more stable in that it changes less as the active space extends. And, for this reason, we use the length gauge in our present work.

Oscillator strengths for the transition $4s^24p-4s4p^2$ ($^2P^o-^2S$ and $^2P^o-^2D$) are listed in Table VI. The other theoretical results are from Aashama *et al.* [39] and Biémont and Quinet [1], while the observed results are from Andersen *et al.* [40],

TABLE VI. Oscillator strengths for $4s^24p-4s4p^2$ ($^2P^o-^2S$ and $^2P^o-^2D$) transitions, (L=length, V=Velocity).

Transition		Ge II	As III	Se IV	Br V	Kr VI
$4s^24p^2P^o-4s4p^2^2S$	This work (CV)	0.676(L)	0.783(L)	0.791(L)	0.817(L)	0.875(L)
		0.682(V)	0.773(V)	0.780(V)	0.800(V)	0.858(V)
	Others	0.684(L) ^a	1.459(L) ^a	0.804(L) ^a	0.741(L) ^a	0.703(L) ^a
		0.583(V) ^a	1.327(V) ^a	0.716(V) ^a	0.671(V) ^a	0.644(V) ^a
$4s^24p^2P^o-4s4p^2^2D$	This work (CV)	0.000(L)	0.213(L)	0.481(L)	0.701(L)	0.802(L)
		0.000(V)	0.198(V)	0.456(V)	0.669(V)	0.791(V)
	Others	0.000(L) ^a	0.306(L) ^a	0.557(L) ^a	0.685(L) ^a	0.785(L) ^a
		0.000(V) ^a	0.303(V) ^a	0.555(V) ^a	0.677(V) ^a	0.759(V) ^a
			0.18 ± 0.018^e	0.45 ± 0.024^c	0.660 ^d	0.791 ^d

^aReference [39].^bReference [40].^cReference [41].^dReference [1].^eReference [42].

TABLE VII. Theoretical and observed lines of Ga-like ions for Rb VII to Nb XI.

Transition	Rb VII		Sr VIII		Zr X		Nb XI	
	Expt.	CV	Expt.	CV	Expt.	CV	Expt.	CV
$4s^2 4p-4s 4p^2$								
$^2P_{1/2}-^2P_{3/2}$	483.277 ^a	482.735	433.746 ^a	433.286	357.583 ^a	357.144	327.442 ^a	327.035
$^2P_{1/2}-^2P_{1/2}$	492.952 ^a	492.212	442.684 ^a	441.977	364.993 ^a	364.332	334.140 ^a	333.532
$^2P_{3/2}-^2P_{3/2}$	508.971 ^a	508.308	460.082 ^a	459.445	384.956 ^a	384.346	355.284 ^a	354.695
$^2P_{3/2}-^2P_{2/2}$	519.771 ^a	518.828	470.155 ^a	469.229	393.553 ^a	392.684	363.171 ^a	362.350
$^2P_{1/2}-^2S_{1/2}$	524.383 ^b	522.950	472.955 ^b	471.734	394.367 ^b	393.432	363.478 ^b	362.661
$^2P_{3/2}-^2S_{1/2}$	554.839 ^b	553.696	504.435 ^b	502.909		426.699		396.991
$^2P_{1/2}-^2D_{3/2}$	622.280 ^b	620.644	555.327 ^b	554.310	454.249 ^b	452.926	414.984 ^b	413.890
$^2P_{3/2}-^2D_{5/2}$	659.071 ^b	657.915	591.833 ^b	590.409	489.866 ^b	488.325	450.021 ^b	448.766
$^2P_{3/2}-^2D_{3/2}$	665.638 ^b	664.423		596.693		497.586		459.210
$^2P_{3/2}-^4P_{5/2}$		828.723		793.919	603.700 ^b	602.574	553.610 ^b	552.602

^aReference [9].

^bReference [15].

Pinnington *et al.* [42], and Bahr *et al.* [41]. The trends of theory and experiment for the $4s^2 4p-4s 4p^2$ case match very

closely, although the relative discrepancy is somewhat larger. The agreement between length and velocity forms of the

TABLE VIII. Wavelength (in Å) for lines in Ga-like ions Yb XL to U LXII.

Ion	Transition	Present			Expt.	Previous
		VV	CV	CC		
Yb XL	$4s^2 4p \ ^2P_{1/2}-4s 4p^2 \ ^2P_{1/2}$	73.075	73.804	73.220	74.22 ^a	72.832
	$4s^2 4p \ ^2P_{1/2}-4s 4p^2 \ ^2D_{3/2}$	74.468	74.463	74.239	74.56 ^a	74.248
Hf XLII	$4s^2 4p \ ^2P_{1/2}-4s 4p^2 \ ^2P_{1/2}$	66.572	66.624	66.510	66.69(3) ^b	66.204
	$4s^2 4p \ ^2P_{1/2}-4s 4p^2 \ ^2D_{3/2}$	67.514	67.547	67.359	67.58(3) ^b	67.334
	$4s^2 4p \ ^2P_{3/2}-4s 4p^2 \ ^2D_{3/2}$	125.37	125.56	124.97	125.64(3) ^b	124.63
	$4s^2 4p \ ^2P_{3/2}-4s 4p^2 \ ^2D_{5/2}$	142.51	142.18	142.01	142.11(3) ^b	141.65
	$4s^2 4p \ ^2P_{3/2}-4s 4p^2 \ ^4P_{3/2}$	157.39	157.11	156.97	157.22(3) ^b	156.48
Ta XLIII	$4s^2 4p \ ^2P_{1/2}-4s 4p^2 \ ^2P_{1/2}$	63.430	63.501	63.338	63.60(2) ^b	63.129
	$4s^2 4p \ ^2P_{1/2}-4s 4p^2 \ ^2D_{3/2}$	64.211	64.313	64.347	64.41(3) ^b	64.141
	$4s^2 4p \ ^2P_{1/2}-4s 4p^2 \ ^4P_{1/2}$	131.57	131.64	131.74	131.68(3) ^b	130.81
	$4s^2 4p \ ^2P_{3/2}-4s 4p^2 \ ^2D_{5/2}$	138.27	138.43	138.78	138.40(3) ^b	137.84
W XLIV	$4s^2 4p \ ^2P_{1/2}-4s 4p^2 \ ^2P_{1/2}$	60.426	60.557	60.523	60.615 7(42) ^c	60.202
	$4s^2 4p \ ^2P_{1/2}-4s 4p^2 \ ^2D_{3/2}$	61.319	61.321	61.163	61.334 1(21) ^c	61.110
	$4s^2 4p \ ^2P_{3/2}-4s 4p^2 \ ^4P_{1/2}$	128.27	128.17	128.13	128.17(4) ^d	127.30
	$4s^2 4p \ ^2P_{3/2}-4s 4p^2 \ ^2D_{5/2}$	135.12	134.83	134.67	134.81(10) ^d	134.20
Os XLVI	$4s^2 4p \ ^2P_{1/2}-4s 4p^2 \ ^2P_{1/2}$	54.984	55.106	55.061	55.123(6) ^e	54.764
	$4s^2 4p \ ^2P_{1/2}-4s 4p^2 \ ^2D_{3/2}$	55.702	55.700	55.573	55.741(5) ^e	55.497
Pt XLVIII	$4s^2 4p \ ^2P_{1/2}-4s 4p^2 \ ^2P_{1/2}$	50.173	50.185	50.199	50.180(4) ^f	49.832
	$4s^2 4p \ ^2P_{1/2}-4s 4p^2 \ ^2D_{3/2}$	50.663	50.678	50.696	50.673(3) ^f	50.428
Au IL	$4s^2 4p \ ^2P_{1/2}-4s 4p^2 \ ^2P_{1/2}$	47.849	47.485	47.809	47.86(5) ^g	47.540
	$4s^2 4p \ ^2P_{1/2}-4s 4p^2 \ ^2D_{3/2}$	48.277	48.276	47.813	48.28(5) ^g	47.603
	$4s^2 4p \ ^2P_{1/2}-4s 4p^2 \ ^4P_{1/2}$	112.91	112.87	112.82	112.81(3) ^b	111.80
Bi LII	$4s^2 4p \ ^2P_{1/2}-4s 4p^2 \ ^2P_{1/2}$	39.604	39.656	39.645	39.690(3) ^e	39.403
	$4s^2 4p \ ^2P_{1/2}-4s 4p^2 \ ^2D_{3/2}$	39.962	39.979	39.894	39.991(3) ^e	39.769
Th LX	$4s^2 4p \ ^2P_{1/2}-4s 4p^2 \ ^2P_{1/2}$	28.623	28.653	28.642	28.677(3) ^e	28.423
	$4s^2 4p \ ^2P_{1/2}-4s 4p^2 \ ^2D_{3/2}$	28.682	28.809	28.664	28.835(3) ^e	28.620
U LXII	$4s^2 4p \ ^2P_{1/2}-4s 4p^2 \ ^2P_{1/2}$	26.153	26.148	26.137	26.147(3) ^e	25.897
	$4s^2 4p \ ^2P_{1/2}-4s 4p^2 \ ^2D_{3/2}$	26.260	26.257	26.223	26.283(3) ^e	26.065

^aReference [18].

^bReference [43].

^cReference [19].

^dReference [21].

^eReference [22].

^fReference [44].

^gReference [23].

calculated gf values is remarkably good. This agreement is slightly spurious in that all gf values reported in this paper are uncorrected for the ratio of the observed to calculated energies. The oscillator strength for the transition $4s^2 4p^2 P^o - 4s 4p^2 ^2S$ of As III from Aashama *et al.* is suspect, because the result is out of the trend and about twice the experimental result.

Spectra of the galliumlike ions Rb VII, Sr VIII, Zr X, and Nb XI emitted from sparks and laser-produced plasmas reported by Litzén and Reader [15] are given in Table VII. The previous experimental results from sparks recorded by Reader *et al.* [9] are also included in Table VII. In our calculation, the wavelengths with CV correlation are found to be close to the experimental results. It is interesting that the maximum difference between the CV results and the experimental results from Reader *et al.* [9] is 0.943 Å (about 0.22%), while the difference between the CV and the results from Litzén and Reader [15] is 1.743 Å. And our results are in general shorter than the results from Litzén and Reader, about 1 Å. Even after considering the uncertainty (0.02 Å), the maximum difference is still up to 0.33%. For this case, we think there are two reasons that need to be considered in the line identifications. First, how are the location and the intensity of the observed calibration lines identified? Second, which models are used for the evolution of the measured spectra? A more detailed introduction to line identification is given in Ref. [43]. Some new line wavelengths are also given in Table VII, which need to be checked in future experiments.

Theoretical and experimental results of wavelengths and transition probabilities for lines in Ga-like ions Yb XL–U LXII are summarized in Ref. [26]. The theoretical results are calculated by using the fully relativistic MCDP approach with the latest version of GRASP. We note that there is a difference of about 0.2~1.4 Å between the theoretical and experimental results. Also, some additional experimental data are available. In order to validate the present model and to make sure that the present calculations are accurate, a comparison of wavelengths for Yb XL–U LXII is presented in Table VIII. The experimental results are given by Fournier *et al.* [18], Utter *et al.* [19], Träbert *et al.* [22,23,44], Ralchenko

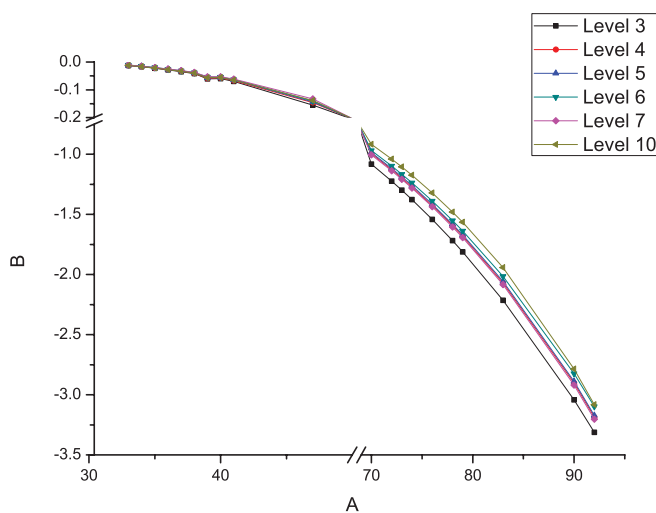


FIG. 2. (Color online) QED to the levels of $4s4p^2$. The level numbers in the figure are the index numbers listed in Table II.

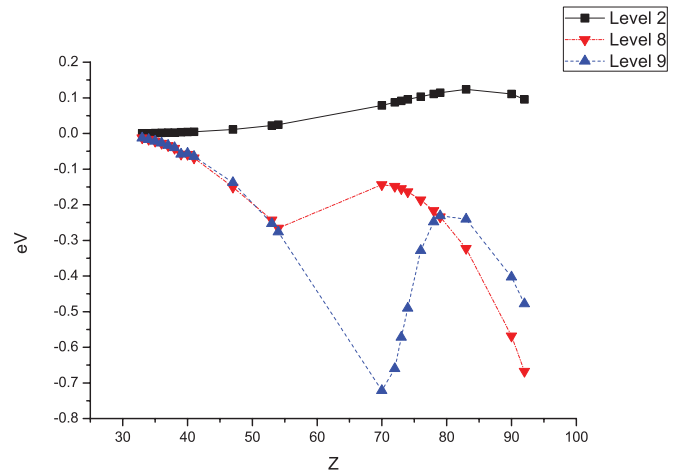


FIG. 3. (Color online) QED to the levels of $4s^2 4p^2$ and $4s 4p^2$. The level numbers in the figure are the index numbers listed in Table II.

et al. [21], and Draganić *et al.* [43]. When comparing the transition probabilities (not listed in this paper) obtained in the length and velocity gauges, we observe a very nice agreement (within 8%) for all the ions considered in the present work, which is similar to the line strengths mentioned above and to the calculation done by Quinet *et al.* [26]. For all ions, it is clear that the calculated values including the CV correlation are in general in very good agreement with the experimental results. Compared with the experimental results, the present CV results are less than 0.05 Å for the most part, except for three transitions (0.416 Å for $4s^2 4p^2 P_{1/2} - 4s 4p^2 ^2P_{1/2}$ of Yb XL, 0.11 Å for $4s^2 4p^2 P_{3/2} - 4s 4p^2 ^4P_{3/2}$ of Hf XLII, and 0.375 Å for $4s^2 4p^2 P_{1/2} - 4s 4p^2 ^2P_{1/2}$ of Au II).

QED corrections are important for high-precision excitation and transition energy calculations, especially for high- Z ions. They are dominated by one-loop radiative corrections from electron self-energy and vacuum polarization. In this work, the QED corrections of each energy level are plotted in the figures. It is obvious that, with increasing element number, the QED corrections become larger. In Fig. 2, the QED corrections to levels 3, 4, 5, 6, 7, and 10 have been given, while the QED corrections to levels 2, 8, and 9 are plotted in Fig. 3. Because of the QED correction to different energy levels, the relations between two states ($4s^2 4p^2 P_{3/2}$ corresponding to level 2 in Fig. 3, and $4s 4p^2 ^4P_{1/2}$ corresponding to level 3 in Fig. 2) have been changed. In the range $Z \geq 74$, the $4s 4p^2 ^4P_{1/2}$ level has been the lowest level relative to the ground state, while the $4s^2 4p^2 P_{3/2}$ level is the lowest for Ge II to Ta XLIII. In order to display the QED correction, the differences have been converted to units of eV. We have used $1 \text{ eV} = 8065.5447 \text{ cm}^{-1}$. From Fig. 2, the QED is found to be up to 3.31 eV for U LXII. It is interesting that the trend of the QED to levels 8 and 9 is not systematic, but the energies of levels 8 and 9 are found to be close to the results calculated by Quinet *et al.* [26].

IV. CONCLUSION

We report on relativistic multiconfiguration Dirac-Fock (MCDP) method of fine-structure energy levels, the term splitting, the wavelengths, and the transition rates of the

Gallium-like $4s^2 4p-4s 4p^2$ transitions in the ions Ge II–U LXII. We show different results for fine-structure energies from methods that include different effects. The MCDF method gives rise to excellent agreement with experimental data and adopted results. It would be beneficial if experimental data for other highly charged Ga-like ions were available. At present, there are no experimental data between $Z \geq 55$ and $Z \leq 92$ for the gallium isoelectronic sequence. The availability of such data would lead to an improved understanding of the relative importance of different contributions to the energies of highly charged ions. The influence of core-valence correlations on the oscillator strengths and wavelengths was discussed. These calculations provide a theoretical benchmark for comparison with experiment and theory. It is found that the relativistic and configuration interaction effects play an important role in the correct assignment of different transitions and also in the accurate evaluation of atomic transition data of highly ionized atoms. For low- to mid- Z ions (see Tables II–IV) it is clear that the MCDF method, including core-valence correlation, is an accurate approach for the whole sequence and that calculations including only valence correlations and core-core correlations underestimate the energy levels. For high- Z ions

(see Tables VII and VIII), the calculated wavelengths including core-valence correlation are in good agreement with the experimental results (about 0.05 \AA). It is in general clear that these kinds of transitions require much work, especially on the experimental side, to explain the differences between different computational methods and to facilitate their use in plasma diagnostics. However, because these results are all from single- or few-configuration calculations, it would be prudent to conclude that more calculations with more configurations are clearly in need. We hope that these results are beneficial in analyzing previous experiments and planning new ones.

ACKNOWLEDGMENTS

The authors are grateful to C. Froese Fisher for providing the GRASPVU package. This work was supported by the National Natural Science Foundation of China (Grant No. 11174213), the National Natural Science Fund (Grant No. 10874156), especially the Science and Technology Foundation of CAEP (Grant No. 2010A0102003). The computational work was carried out on the cluster at the Research Center of Laser Fusion, CAEP.

-
- [1] É. Biémont and P. Quinet, *J. Quant. Spectrosc. Radiat. Transfer* **44**, 233 (1990).
- [2] C. J. Budhiraja and Y. N. Joshi, *Can. J. Phys.* **49**, 391 (1971).
- [3] E. Alexander, M. Even-Zohar, B. S. Frankel, and S. Goldsmith, *J. Opt. Soc. Am.* **61**, 508 (1971).
- [4] M. Druetta and J. Buchet, *J. Opt. Soc. Am.* **66**, 433 (1976).
- [5] M. Finkenthal, R. E. Bell, H. W. Moos, A. K. Bhatia, E. S. Marmar, J. L. Terry, and J. E. Rice, *Phys. Lett. A* **82**, 123 (1981).
- [6] M. A. Khan, *J. Opt. Soc. Am.* **72**, 268 (1982).
- [7] P. Audebert, J. C. Gauthier, J. P. Geindre, C. Chenais-Popovics, C. Bauche-Arnoult, M. Klapisch, E. Luc-Koeing, and J. F. Wyart, *Phys. Rev. A* **32**, 409 (1985).
- [8] B. Denne, E. Hinnov, S. Cohen, and J. Timberlake, *J. Opt. Soc. Am. B* **2**, 1661 (1985).
- [9] J. Reader, N. Acquista, and S. Goldsmith, *J. Opt. Soc. Am. B* **3**, 874 (1986).
- [10] E. H. Pinnington, J. A. Kernahan, and K. E. Donnelly, *J. Opt. Soc. Am.* **67**, 162 (1977).
- [11] D. J. G. Irwin, J. A. Kernahan, E. H. Pinnington, and A. E. Livingston, *J. Opt. Soc. Am.* **66**, 1396 (1976).
- [12] A. E. Livingston, *J. Phys. B* **9**, L215 (1976).
- [13] E. H. Pinnington, *Beam-Foil Spectroscopy* (Plenum, New York, 1976), Vol. 1, p. 235.
- [14] E. Träbert, G. Möller, A. E. Livingston, and P. H. Heckmann, *Atomic Spectra and Oscillator Strengths for Astrophysics and Fusion Research*, edited by J. E. Hansen (Elsevier, Amsterdam, 1990), p. 180.
- [15] U. Litzéz and J. Reader, *Phys. Scr.* **39**, 73 (1989).
- [16] J. G. Li, E. Träbert, and C. Z. Dong, *Phys. Scr.* **83**, 015301 (2011).
- [17] Y. Ishikawa and M. J. Vilkas, *Phys. Rev. A* **77**, 052701 (2008).
- [18] K. B. Fournier, W. H. Goldstein, A. Osterheld, M. Finkenthal, S. Lippmann, L. K. Huang, H. W. Moos, and N. Spector, *Phys. Rev. A* **50**, 2248 (1994).
- [19] S. B. Utter, P. Beiersdorfer, and E. Träbert, *Can. J. Phys.* **80**, 1503 (2002).
- [20] T. Pütterich, R. Neu, C. Biedermann, R. Radtke, and ASDEX Upgrada Team, *J. Phys. B: At. Mol. Opt. Phys.* **38**, 3071 (2005).
- [21] Y. Ralchenko, J. Reader, J. M. Pomeroy, J. N. Tan, and J. D. Gillaspay, *J. Phys. B: At. Mol. Opt. Phys.* **40**, 3861 (2007).
- [22] E. Träbert, P. Beiersdorfer, K. B. Fournier, and M. H. Chen, *Can. J. Phys.* **83**, 829 (2005).
- [23] E. Träbert, P. Beiersdorfer, K. B. Fournier, S. B. Utter, and K. L. Wong, *Can. J. Phys.* **79**, 153 (2001).
- [24] K. B. Fournier, *At. Data Nucl. Data Tables* **68**, 1 (1998).
- [25] U. I. Safronova and A. S. Safronova, *J. Phys. B: At. Mol. Opt. Phys.* **43**, 074026 (2010).
- [26] P. Quinet, É. Biémont, P. Palmeri, and E. Träbert, *At. Data Nucl. Data Tables* **93**, 167 (2007).
- [27] Norrington, [<http://www.am.qub.ac.uk/DARC>].
- [28] L. H. Hao, G. Jiang, and H. J. Hou, *Phys. Rev. A* **81**, 022502 (2010).
- [29] F. Hu, G. Jiang, J. M. Yang, C. K. Wang, X. F. Zhao, and L. H. Hao, *Eur. Phys. J. D* **61**, 15 (2011).
- [30] I. P. Grant, *Quantum Theory of Atoms and Molecules* (Springer, New York, 2007), p. 393.
- [31] F. A. Parpia, C. Froese Fischer, and I. P. Grant, *Comput. Phys. Commun.* **94**, 249 (1996).
- [32] Y. K. Kim, D. H. Baik, and P. Indelicato, *Phys. Rev. A* **44**, 148 (1991).
- [33] P. J. Mohr, *Phys. Rev. Lett.* **34**, 1050 (1975); *Phys. Rev. A* **26**, 2338 (1982).
- [34] W. R. Johnson and G. Soff, *At. Data. Nucl. Data Tables* **33**, 405 (1985).

- [35] L. W. Fullerton and G. A. Rinker Jr., *Phys. Rev. A* **13**, 1283 (1976).
- [36] J. Olsen, M. R. Godefroid, P. A. Jonsson, P. A. Malmquist, and C. Froese Fischer, *Phys. Rev. E* **52**, 4499 (1995).
- [37] Y. Ralchenko, A. E. Kramida, J. Reader, and NIST ASD Team, NIST Atomic Spectra Database (ver. 4.0.1) (National Institute of Standards and Technology, Gaithersburg, MD, 2010), [http://physics.nist.gov/PhysRefData/ASD/levels_form.html].
- [38] A. Tauheed and Y. N. Joshi, *Phys. Scr.* **80**, 025305 (2009).
- [39] K. Aashama, T. M. Luke, and J. D. Talman, *J. Phys. B: At. Mol. Phys* **16**, 2695 (1983).
- [40] T. Andersen and A. Lindgård, *J. Phys. B: At. Mol. Phys* **10**, 2359 (1977).
- [41] J. L. Bahr, E. H. Pinnington, J. A. Kernahan, and J. A. O'Neill, *Can. J. Phys.* **60**, 1108 (1982).
- [42] E. H. Pinnington, J. L. Bahr, J. A. Kernahan, and D. J. G. Irwin, *J. Phys. B: At. Mol. Phys* **14**, 1291 (1981).
- [43] I. N. Draganić, Y. Ralchenko, J. Reader, J. D. Gillaspay, J. N. Tan, J. M. Pomeroy, S. M. Brewer, and D. Osin, *J. Phys. B: At. Mol. Opt. Phys.* **44**, 025001 (2011).
- [44] E. Träbert, J. Clementson, P. Beiersdorfer, J. A. Santana, and Y. Ishikawa, *Phys. Rev. A* **82**, 062519 (2010).